ELSEVIER

International Journal of Mass Spectrometry 219 (2002) 325–341

International Journal of Mass Spectrometry

www.elsevier.com/locate/ijms

Some properties of charged particle trajectories in quadrupole mass spectrometers Part II. The results of trajectory analysis

Ernst P. Sheretov*, Igor V. Philippov, Tatiana B. Karnav, Edgar V. Fedosov, Vladimir W. Ivanov

Department of Physics, Ryazan State Radio Technical University, Gagarin street 59/1, 391000 Ryazan, Russia

Received 28 January 2002; accepted 29 May 2002

Abstract

In this article, we show that the dependence of the amplitude of ion oscillation within hyperboloidal mass spectrometers (QMSs) on the stability parameter β_0 has a "spiking" structure: the amplitude vs. the stability parameter β_0 curve exhibits narrow dips at some points. We show that the dips appear at those points of the stability diagram that lie on quasi-stability lines; that is to say the novel spiking structure of the observed amplitude vs. β_0 curve is determined by fine structure of the stability diagram.

We have found that the amplitude-phase characteristic (APC) of the first kind has a plateau with amplitude equal to 1 at the points lying at quasi-stability lines. Trajectory analysis demonstrates an one-to-one correspondence (for meander and $\beta_0 = 0$) of the APC of the first and second kinds with the theory developed in Part I of this article. The shape of the dips discovered in this work was investigated. The width of these dips depends on the exposure time (the time that ions are exposed to the rf field). For the exposure time that exceeds 100 rf cycles, the width of the dips can be characterized in terms of "resolution" ($a_2^2/\Delta a_2^2$) of about several hundreds. We show that the smooth component of the amplitude vs. β_0 curve is described precisely by Eq. (14) developed in Part I. (Int J Mass Spectrom 219 (2002) 325–341)

Keywords: Mass spectrometry; Hill equation; Ion trap; Ion trap mass spectrometry

1. Introduction

In the development of quadrupole mass spectrometry and, in particular, those instruments that utilize three-dimensional ion traps, there is intense interest in the investigation of trapping ions injected into an electric rf field. Now, attempts to find effective external ion injection methods are especially important. The utilization of such methods could improve substantially analytical characteristics and parameters of ion trap mass spectrometers and to permit the implementation of those advantages that have not yet been exploited fully.

The problem of ion injection can be tackled successfully by the sequential development of a linear model: first of all, developing the fundamental theory of solutions of the Hill equation and, secondly, investigating the properties of ion trajectories.

This work is a continuation of a series of our articles published in recent years and describing

* Corresponding author. E-mail: sheretov@eac.ryazan.su

1387-3806/02/$ – see front matter
PII S1387-3806(02)00739-X

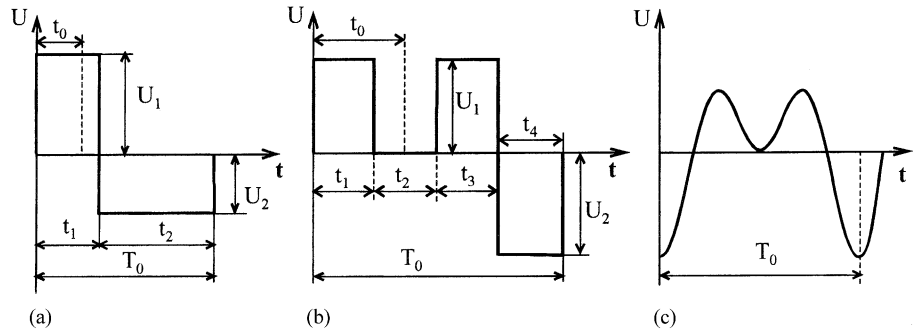

Fig. 1. Waveforms of the rf voltage used in the work: (a) a simple rectangular waveform; (b) pulsed EC-signal; (c) harmonic EC-signal.

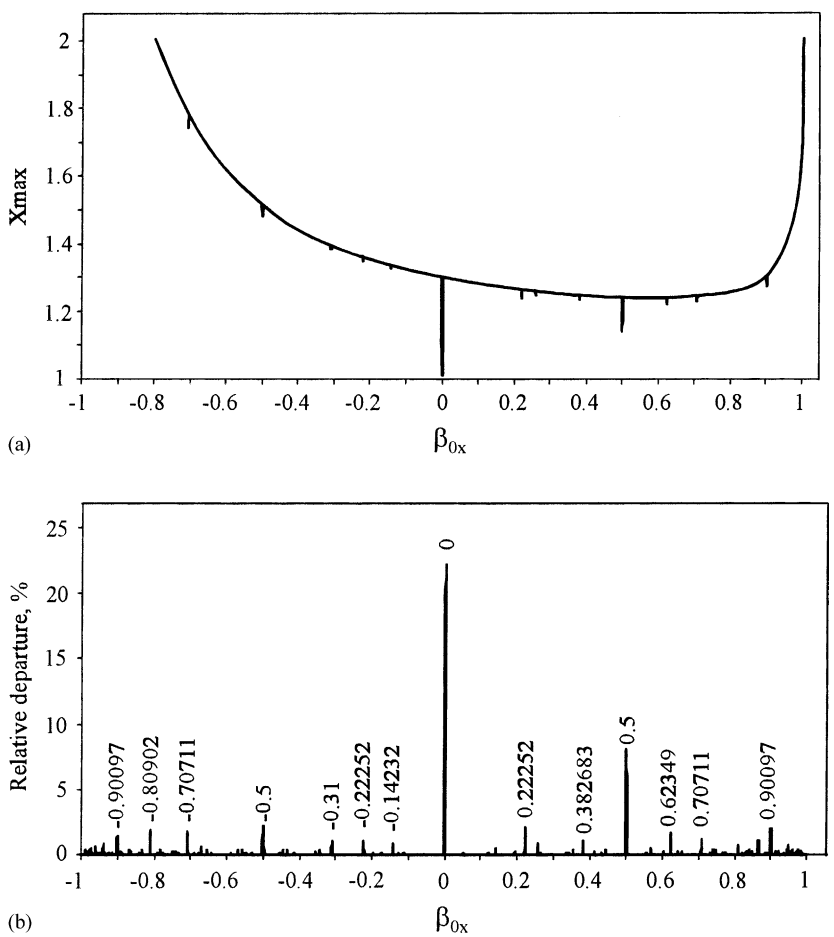

Fig. 2. The variation of the oscillation amplitude as a function of working point location on the stability diagram calculated for the "meander" (a 50% duty-cycle symmetric rectangular waveform): (a) the oscillation amplitude vs. the stability parameter β_0; (b) the relative departure of the amplitude of each dip from the amplitude at the smooth component of the amplitude vs. β_0 curve.

Table 1
Amplitude of ion oscillation at the dips and at the smooth component of the amplitude vs. β_0 curve for various initial phases

Phase	0.18	0.2	0.22	0.24	0.251	0.26	0.28	0.3	0.32	0.35	0.375	0.39	0.42	0.498	0.51	0.53
x_{dip}	1.83	1.59	1.34	1.077	1.029	1.036	1.05	1.065	1.081	1.103	1.122	1.133	1.156	1.214	1.18	1.118
x_{smooth}	1.88	1.68	1.48	1.3	1.22	1.23	1.24	1.25	1.26	1.27	1.28	1.29	1.3	1.37	1.28	1.14
Δx (%)	2.7	5.6	10.4	20.7	18.5	18.7	18.1	17.4	16.5	16	14.9	14.7	14.2	12.8	8.4	2
$(x_{smooth} - 1)/x_{dip}$	1.06	1.15	1.41	3.9	7.58	6.4	4.8	3.84	3.21	2.72	2.37	2.25	2.05	1.73	1.55	1.18

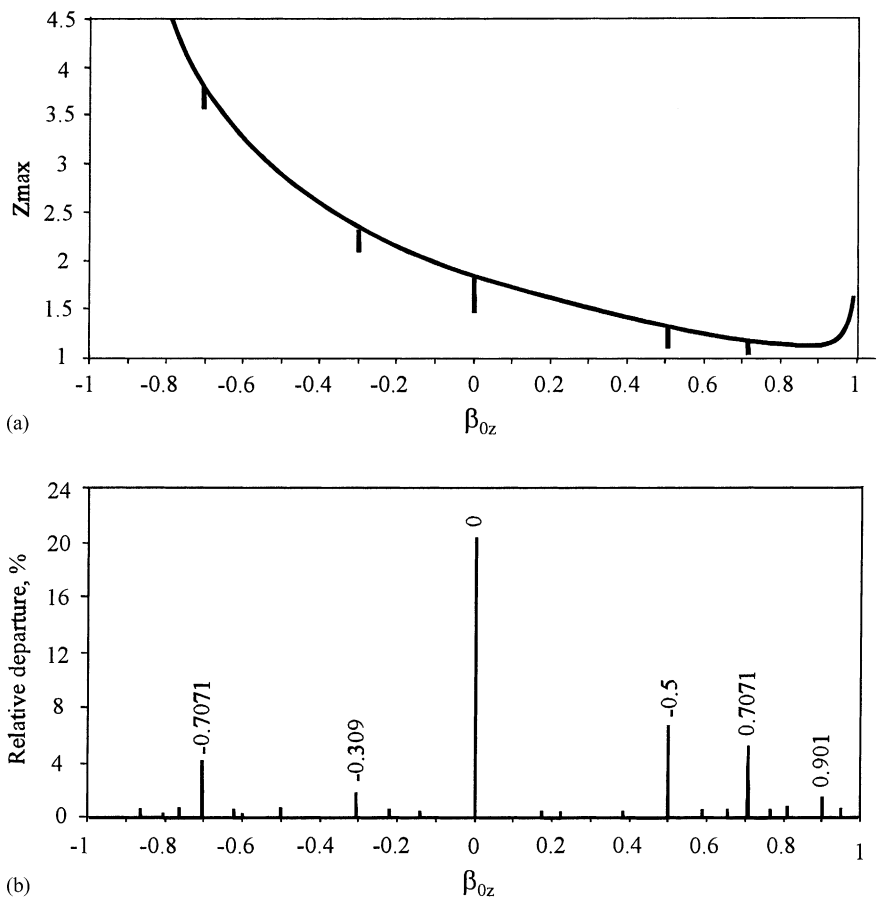

Fig. 3. The variation of the oscillation amplitude as a function of working point location on the stability diagram calculated for the rf voltage of harmonic waveform. Ions were injected along the Z axis: $z_0 = 1$; the initial energy is 5 eV; the slope of the scan line is $\lambda = 0$ (zero dc voltage); the initial phase is $t_0 = 0.25$: (a) the oscillation amplitude vs. the stability parameter β_0; (b) the relative departure of the amplitude of each dip from the amplitude at the smooth component of the amplitude vs. β_0 curve.

various aspects of mass spectrometry [1–5]. In this article, we investigate some properties of ion trajectories within quadrupole mass spectrometers and show the dependence of the amplitude of ion oscillations on the working point location in the stability diagram.

2. The amplitude of the oscillatory ion motion vs. the working point location in the stability diagram

Investigations were carried out using software developed in our laboratory for various rf waveforms applied to the electrodes of the ion trap: harmonic voltage, pulsed EC-signal, voltage with rectangular waveform—"meander" (a 50% duty-cycle symmetric rectangular waveform) and harmonic EC-signal [4,5]. The periods of the rf voltages used in the work are shown in Fig. 1.

The amplitudes of ion oscillations were determined by direct trajectory calculations using traditional techniques. Ion trajectories along different coordinate axes were analyzed for various initial phases, initial coordinates and velocities. Working points lying on different scan lines were chosen, with emphasis on the scan line that corresponds to the driving rf voltage with zero dc component.

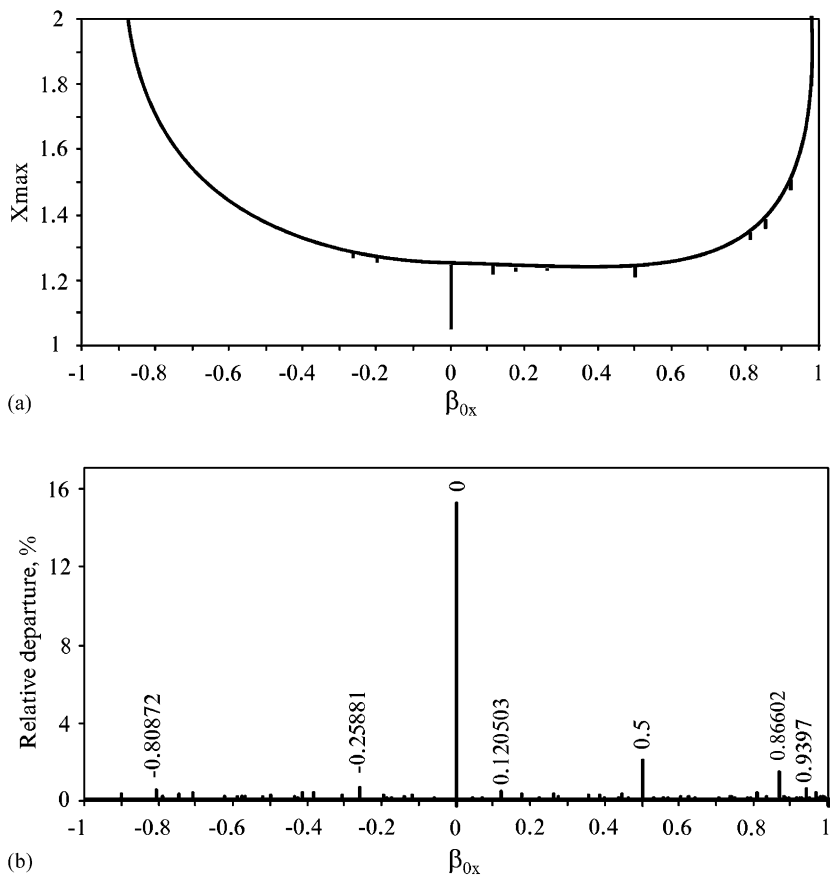

Fig. 4. The variation of the oscillation amplitude as a function of working point location on the stability diagram calculated for the pulsed EC-signal. Ions were injected along the X axis: $x_0 = 1$; initial energy is 5 eV; the slope of the scan line is $\lambda = 0.707106781$ (zero dc voltage); the initial phase is $t_0 = 0.25$: (a) the oscillation amplitude vs. the stability parameter β_0; (b) the relative departure of the amplitude for each dip from the amplitude at the smooth component of the amplitude vs. β_0 curve.

A requirement of an effective external ion injection simulation method is the ability to calculate the maximum ion excursion from the origin of coordinates with a high accuracy of about 10^{-3}%.

A typical dependence of the oscillation amplitude as a function of working point location in the stability diagram is shown in Fig. 2. In this figure, X_{max} is the extremal ion excursion from the origin normalized to the initial coordinate. The curve shown in Fig. 2a was calculated for a pulse voltage of rectangular waveform "meander" (see Fig. 1a): $t_1 = t_2$, $\lambda = U_1/U_2 = 1$ (zero dc component); $U_{p-p} = 1000$ V; the initial phase, measured from the beginning of the focusing pulse, is $t_0 = 0.25$ (optimal phase of the first kind). The ion oscillates along the X axis; the initial coordinates are $x_0 = 1$; $y_0 = 0$; $z_0 = 0$; the initial velocity $\dot{x}_0$ corresponds to an energy of 5 eV; $\dot{y}_0 = 0$ and $\dot{z}_0 = 0$. From Fig. 2a, we see that the amplitude vs. the stability parameter β_0 curve exhibits a spiking structure. This dependence represents a smooth curve (component) with narrow dips or inverted peaks at some values of β_0. The depth of each dip varies according to the rf voltage waveform, and initial parameters of ion motion (injection phase t_0, etc.). Only one characteristic

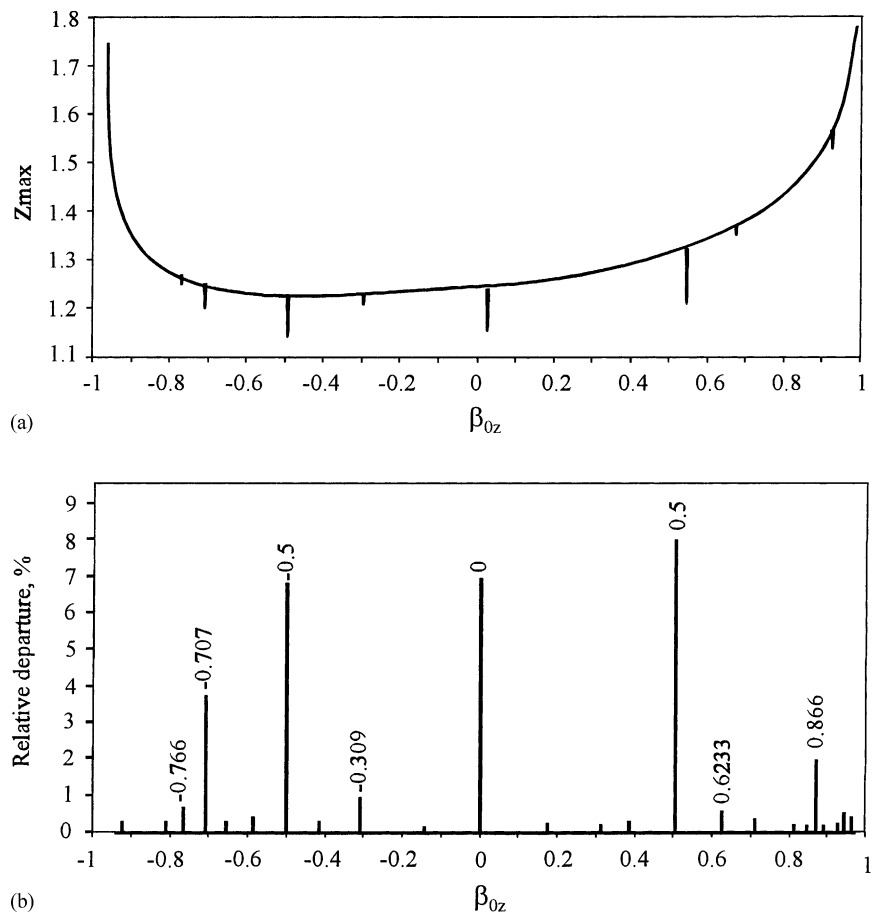

Fig. 5. The variation of the oscillation amplitude as a function of working point location on the stability diagram calculated for the harmonic EC-signal. Ions were injected along the Z axis: $z_0 = 1$; the initial energy is 5 eV; the slope of the scan line is $\lambda = 0$ (zero dc voltage); $t_0 = 0.1666$: (a) the oscillation amplitude vs. the stability parameter β_0; (b) the relative departure of the amplitude for each dip from the amplitude at the smooth component of the amplitude vs. β_0 curve.

is unchangeable—the position of the dips on the β_0 axis. Fig. 2b shows the relative departure of the amplitude for each dip from the amplitude at the smooth component of the amplitude vs. β_0 curve. The more intense peaks in this figure have been identified by the respective values of the β_0 stability parameter. All of the β_0 values shown in this figure can be found in Table 1 presented in Part I of this article. This means that the observed amplitude excursion occurs for those working points that lie on quasi-stability lines. The analogous curves, obtained for an harmonic voltage, pulse EC-signal and harmonic EC-signal, are shown in Figs. 3–5, respectively. Comparing Figs. 2–5, we notice that the maximum relative depth of the dips is observed for $\beta_0 = 0$, 0.5 and -0.5. Only the data obtained with the harmonic EC-signal yield dips of similar depth for these three values of β_0 (Fig. 5). For the other waveforms, we obtain the deepest dip for $\beta_0 = 0$: for the rectangular waveform, the dip depth is greater by a factor of about 7 (Fig. 4); for "meander" (Fig. 2) and the harmonic EC-signal (Fig. 3), the dip depth for $\beta_0 = 0$ is greater approximately by a factor of 3 than those for $\beta_0 = \pm 0.5$.

As discussed above, the intensity of the dips depends on the initial conditions of ion motion. Fig. 6 illustrates the influence of initial phase on ion trajectory amplitude vs. stability parameter curve calculated for the "meander" waveform; the working points lay on the scan line of slope $\lambda = 1$. Curve 1 in this figure was calculated for the initial phase $t_0 = 0.25$, curve 2 corresponds to $t_0 = 0.275$. We see that the initial phase affects both the character of the smooth component of the curves and the relative magnitudes of the dips for $\beta_{0x} = 0$, 0.5 and -0.5. We have investigated also the influence of initial energy and the storage time on behavior of the oscillation amplitude in the vicinity of the dips. An increase in the initial velocity increases the amplitude and the relative depth of the dips in all points ($\beta_0 = 0$ and $\beta_0 = \pm 0.5$). The exposure time has no influence on the oscillation amplitude at the dips for the case where it exceeds 5–10 rf cycles. One can understand this fact because $i = 2$ for $\beta_0 = 0$ and $i = 3$ for $\beta_0 = \pm 0.5$. The amplitude of ion oscillations at $\beta_0 = 0$ is nearly constant in the neighborhood of the optimal phase of the first kind. However, the relative depth here depends on the phase. If the working points locate at $\beta_0 = \pm 0.5$ then the phase variation changes both amplitude and relative depth of the dips.

The data listed in Table 1 illustrates oscillation amplitude along the X axis and the relative depth of the dips at $\beta_{0x} = 0$ as a function of the initial phase calculated for the pulse EC-signal ($t_1 = t_2 = t_3 = t_4 = 0.25$, see Fig. 1b). The initial velocity $\dot{x}_0$ of the injected ion corresponds to an energy of 5 eV.

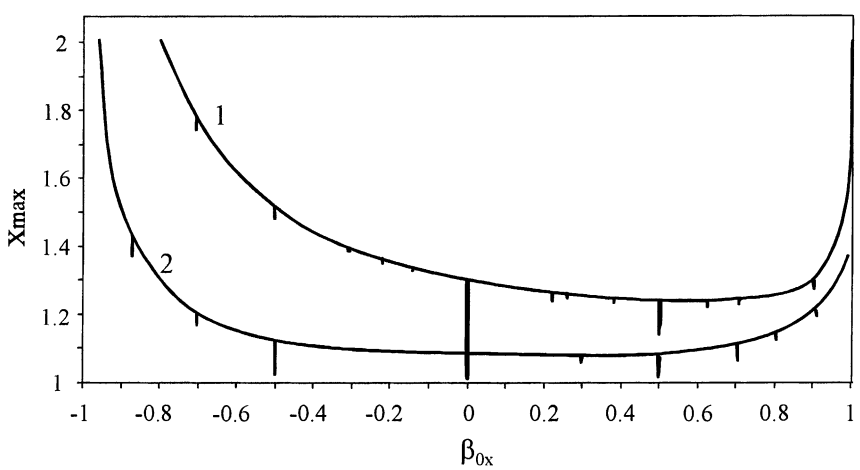

Fig. 6. The influence of initial phase on the amplitude of ion oscillations vs. stability parameter curve calculated for the "meander" waveform: (1) $t_0 = 0.25$; (2) $t_0 = 0.275$.

The slope of the scan line $\lambda = 0.707106781$ corresponds to zero dc component of the rf voltage. The range of phases presented in Table 1 covers the first and second focusing pulses partially and the entire active part of the EC-signal. In this table, x_{dip} represents oscillation amplitude at the dips; x_{smooth} represents the amplitude out of the dips; Δx is the relative depth of the dips. It can be seen that the relative depth is maximal at the end of the first focusing pulse (near the optimal phase of the first kind), the depth remains relatively high within the active part up to the beginning of the second focusing pulse (again, here the optimal phase of the first kind is located) and then decreases.

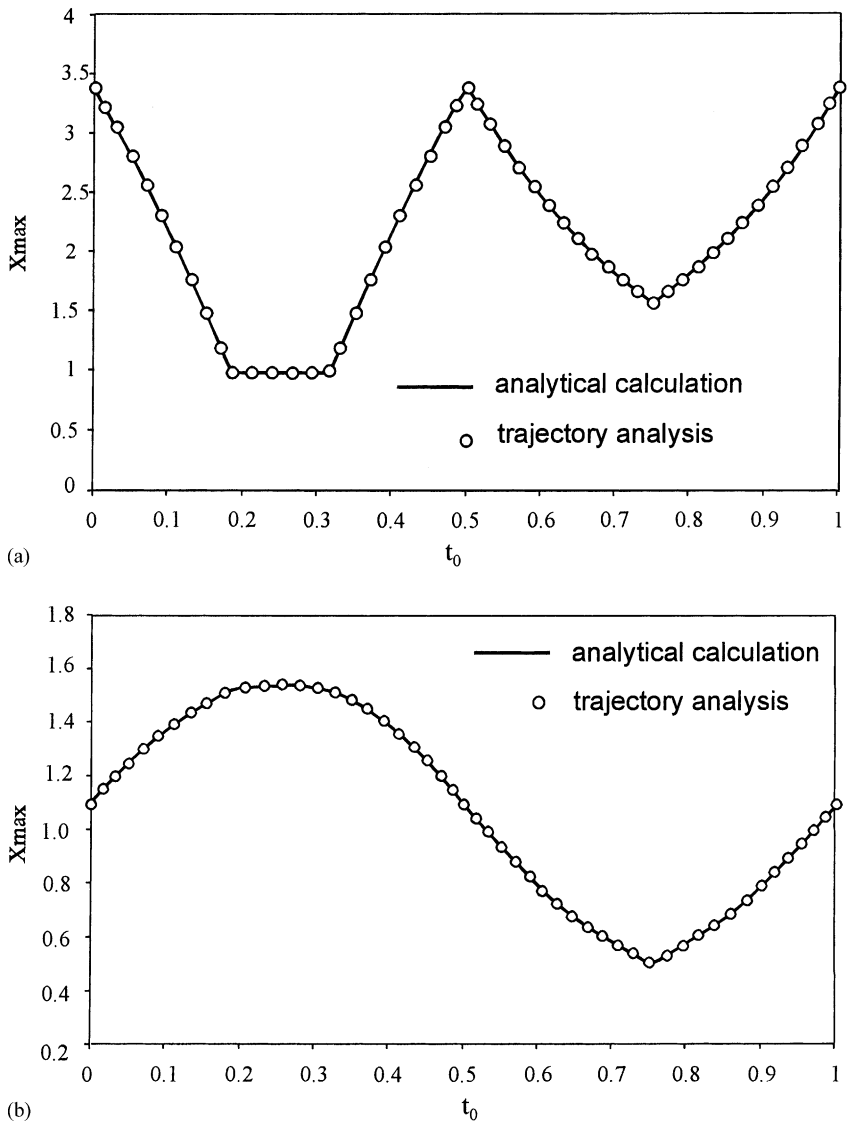

Fig. 7. The dependence of oscillation amplitude on the initial phase in the case of "meander": (a) amplitude-phase characteristic of the first kind; (b) amplitude-phase characteristic of the second kind. Solid lines represent amplitude of ion oscillation obtained from analytical expressions; datum points correspond to results of the trajectory analysis.

The presence of the dips in the amplitude vs. the stability parameter curve is very important for the trapping of externally generated ions. In fact, a maximum excursion of the injected ion (normalized to the initial coordinate) is always greater than 1. The maximum displacement is equal to 1 only at the optimal phase of the first kind and if initial velocity is equal to zero. This is a well-known theoretical restriction for one-dimensional injection of ions created externally into the rf field of the ion trap. However, it is possible to overcome this theoretical "taboo" and several methods to do it are known. These are:

- The use of aperiodic solutions of the Hill equation (β_0 is an irrational quantity [6,7]).
- The use of ion motion along other coordinate axes (different to the injection axis). In this case an ion is shifted along another coordinate axis and reaches its extremum coordinate in a region of the analyzer with a greater distance between this axis and electrode surface. For example, an ion is injected through the ring electrode in the radial plane. The injection coordinate is equal to a minimum radius of the ring electrode. If the ion is shifted in the z direction then the distance from the Z axis and the ring electrode increases because of the electrode profile.
- The use of collisions with buffer gas molecules.
- The use of non-linear field distortions caused either by electrode surface imperfections, a boundary region, or channels for injection/ejection of ions.

Let us assume that negotiation of the theoretical restriction depends on the difference between maximum ion displacement and 1: $\Delta Y_\mathrm{m} = Y_\mathrm{m} - 1$. If $\Delta Y_\mathrm{m} = 0$ then the restriction is eliminated; if the value of ΔY_m increases then the probability to overcome the theoretical "taboo" decreases (the trapping efficiency decreases also). As an approximation, we can consider the trapping efficiency to be proportional to ΔY_m and then use this parameter to carry out a further comparison. The bottom row in Table 1 gives the ratio between the respective values of ΔY_m determined from the first two rows. If we accept this approximation, then we should expect an increase in the trapping efficiency by a factor of 7 or more for the working points lying on the $\beta_{0x} = 0$ quasi-stability line for the case of the pulse EC-signal.

3. Amplitude-phase characteristics of the first and second kinds for an ion whose working point lies on a quasi-stability line

Theoretical expressions for APC of the first and second kinds were obtained in Part I of this article for "meander" and $\beta_0 = 0$. These are Eqs. (41), (42), (46)

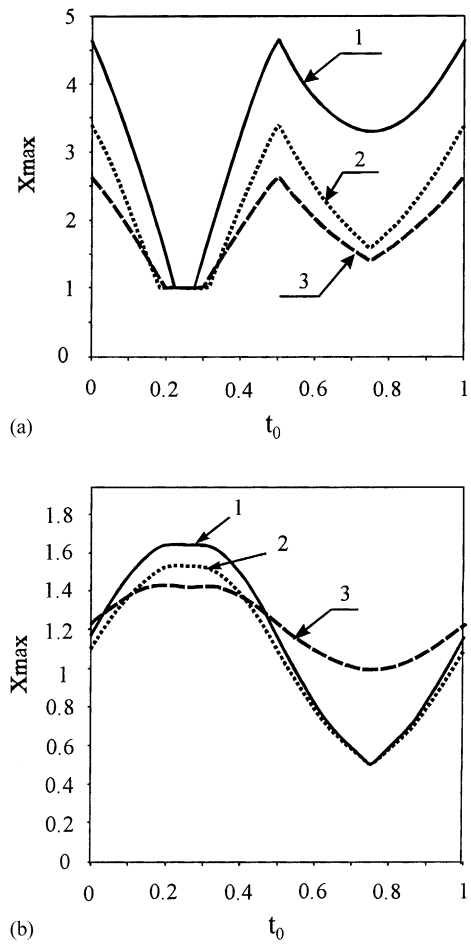

Fig. 8. The oscillation amplitude as a function of the initial phase obtained from trajectory analysis for different values of the stability parameter β_0. The rf waveform—"meander": (a) amplitude-phase characteristic of the first kind; (b) amplitude-phase characteristic of the second kind.

for the APC of the first kind and Eqs. (51)–(53) for the APC of the second kind. In Fig. 7, we compare both characteristics calculated for the meander using the equations obtained (solid line) and direct trajectory calculations (datum points). Calculations were carried out for the working point lying at the intersection of the scan line $\lambda = 1$ with the $\beta_{0x} = 0$ quasi-stability line ($a_1 = a_2 = 3.14158$). We see that the analytical calculation fits perfectly with the results of trajectory analysis. Fig. 8 shows the APC of the first (Fig. 8a) and second (Fig. 8b) kinds obtained from the trajectory analysis. Trajectories were calculated for the meander during 300 rf cycles for the following working points: $a_1 = a_2 = 3.483277$, $\beta_{0x} = -0.5$ (curve 1); $a_1 = a_2 = 3.14158$, $\beta_{0x} = 0$ (curve 2); and $a_1 = a_2 = 2.636899$, $\beta_{0x} = 0.5$ (curve 3). Amplitude-phase characteristics for the x and z coordinates determined from the trajectory calculations for the case of the harmonic waveform are shown in Fig. 9. Curves, labeled 1 in Fig. 9a and b, correspond to $\beta_{0x} = -0.5$ ($a = 0, q = 0.78468$), curves 2 correspond to $\beta_{0x} = 0$ ($a = 0$, $q = 0.63931$), curves 3 were obtained for

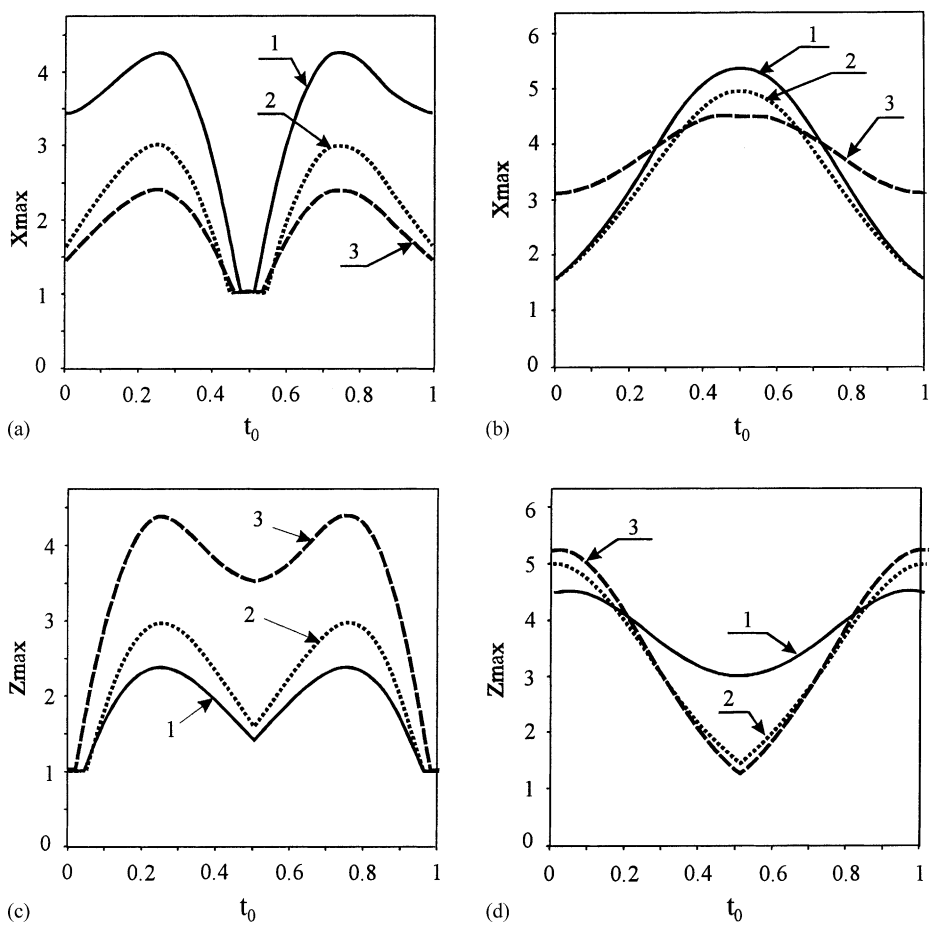

Fig. 9. The oscillation amplitude as a function of the initial phase obtained from trajectory analysis for different values of the stability parameter β_0. The rf voltage of harmonic waveform ($\lambda = 0$): (a) amplitude-phase characteristic of the first kind for the x coordinate; (b) amplitude-phase characteristic of the second kind for the x coordinate; (c) amplitude-phase characteristic of the first kind for the z coordinate; (d) amplitude-phase characteristic of the second kind for the z coordinate; (1) $\beta_{0x} = -0.5$; (2) $\beta_{0x} = 0$; (3) $\beta_{0x} = 0.5$.

$\beta_{0x} = 0.5$ ($a = 0$, $q = 0.4511$). In Fig. 9c and d, curves 1 were calculated for $\beta_{0z} = -0.5$ ($a = 0$, $q = 0.39234124$), curves 2 correspond to $\beta_{0z} = 0$ ($a = 0$, $q = 0.31965744$) and curves 3 were found for $\beta_{0z} = 0.5$ ($a = 0$, $q = 0.22555226$).

Amplitude-phase characteristics of the first and second kinds were also obtained for the harmonic EC-signal (Fig. 10) and for the pulse EC-signal (Fig. 11). From Figs. 8–10, we see that the structures of the amplitude-phase characteristics for all waveforms are similar to the characteristic of the pulse EC-signal in that they have a wide region with amplitude equal to 1. This region governs the effective trapping of slow ions within mass analyzers. It is interesting to note that for $\beta_{0z} = 0$ and $\beta_{0z} = \pm 0.5$, this region is greater than the duration of the active part of the pulse EC-signal. For $\beta_0 = 0$, this effect is more marked.

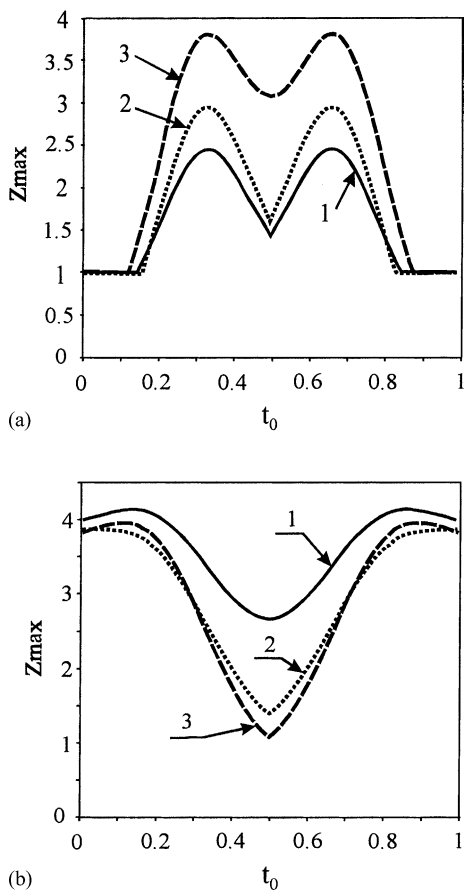

Fig. 10. Amplitude-phase characteristic for the harmonic EC-signal ($\lambda = 0$) obtained from trajectory analysis for different values of the stability parameter β_0: (a) amplitude-phase characteristic of the first kind; (b) amplitude-phase characteristic of the second kind; (1) $\beta_{0x} = -0.5$; (2) $\beta_{0x} = 0$; (3) $\beta_{0x} = 0.5$.

It was shown in Part I of this article that amplitude-phase characteristics of the first kind ("meander"), for working points in the neighborhood of $\beta_0 = 0$, lie above analogous curves determined exactly at $\beta_0 = 0$ (an exception is one phase only—the optimal phase of the first kind). The calculations that we carried out showed the same effect for other rf waveforms. Thus, quasi-stability lines lie within zones having high trapping efficiency for slow ions (it is more correct to say that these zones are located along quasi-stability lines). Any scan line intersects a variety of quasi-stability lines. This results in either irregular shapes of mass peaks (dips in mass peaks) when the ion trap is operated in the mass-selective ion storage mode or causes sensitivity fluctuations within a mass range when the trap is operated in the mass-selective instability mode. In the latter case, the slope of the scan line must affect irregularities of sensitivity throughout the mass range. Thus, we can reach an important conclusion: a linear theory of quadrupole mass spectrometers points to irregularities in the efficiency of the ion trapping within a mass range. This effect is attributed to the fine structure of the stability diagram and the presence of quasi-stability lines within it. In this case, an interpretation of the dips in the mass peaks as a result of non-linear field distortions warrants some additional discussion. Furthermore, we have shown previously in [8] that non-linear field distortions cause instability bands to appear near quasi-stability lines.

Comparing amplitude-phase characteristics of the second kind for points lying on and near quasi-stability lines, we see that the first ones lie under the second. This means that the trapping efficiency for ions having greater velocities (and for slow ions also) is higher for points located on quasi-stability lines. For example, for the "meander" waveform and $\beta_0 = 0$, this conclusion follows from a comparison of amplitude-

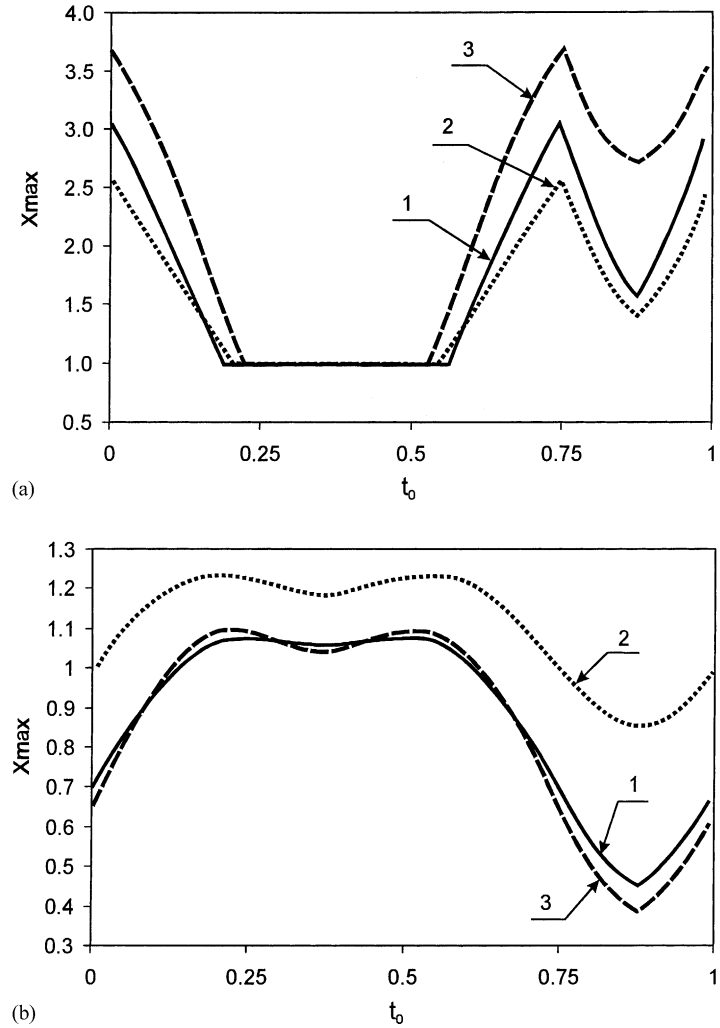

Fig. 11. Amplitude-phase characteristic for the pulse EC-signal, $\lambda = 0.707106781$ (zero dc component), obtained from trajectory analysis for different values of the stability parameter β_0: (a) amplitude-phase characteristic of the first kind; (b) amplitude-phase characteristic of the second kind; (1) $\beta_{0x} = -0.5$; (2) $\beta_{0x} = 0$; (3) $\beta_{0x} = 0.5$.

phase characteristics of the second kind described by Eqs. (49), (51) and (52) in Part 1. It is easy to show that the amplitude-phase characteristics of the second kind have the same maximum values at the optimal phase of the first kind:

$$Y_{\mathrm{m}}^2|_{(0,1)} = \frac{1}{\pi^2}\exp(\pi).$$

At all the other initial phases, the APC of the second kind described by Eq. (14) lies above the analogous characteristics determined by Eqs. (51) and (52) in Part I of this article. At the optimal phase of the second kind, the APC of the second kind reaches its minimum (a phase at which the trapping efficiency of fast ions is maximal) and the value of $Y_{\mathrm{m}}^2|_{(0,1)}$ in the point on the $\beta_0 = 0$ quasi-stability line is a half as large in comparison with points lying near this line.

Ions, created externally, are injected into the ion trap having considerable relative initial coordinates and velocities. In this case, the trapping efficiency

is determined by amplitude-phase characteristics of both first and second kinds. As we mentioned above, the trapping efficiency can be increased by locating working points of the injected ions on quasi-stability lines. This effect is intensified for those points of the stability diagram where quasi-stability lines for different coordinate axes intersect each other. However, the final result depends on a method used to avoid the theoretical restriction imposed on the ion trapping.

4. Profile of the dips observed in the amplitude vs. β_0 curve

Our investigations of the dips observed in the amplitude vs. the stability parameter β_0 curve for working points lying on quasi-stability lines showed that there are some profile features common to all dips. If the smooth curve (described by Eq. (14) in the first part of the article) is parallel to the β_0 axis, then the dips have a symmetric shape with a plateau at the bottom. The working point corresponding to $\beta_0 = 0$ always lies within this plateau. This point is located at one edge of the plateau. The amplitude increases sharply out of the plateau and tends to the respective value of the amplitude on the smooth component of the amplitude vs. β_0 curve.

The behavior of the smooth curve along the β_0 axis varies, but the plateaux of the dips are observed to be nearly parallel to this smooth curve. Fig. 12 illustrates a typical profile of the dips obtained for the pulse EC-signal ($t_1 = t_2 = t_3 = t_4 = 0.25$, $U_{p-p} = 1000$ V) for different initial phases within 100 rf cycles. The slope of the scan line is $\lambda = 0.707106781$ (zero dc voltage); an ion was injected along the X axis with initial energy of 5 eV. The curves in Fig. 12 were calculated for working points located near the quasi-stability line of $\beta_{0x} = 0$. Fig. 13 shows that the dips in the amplitude vs. the stability parameter β_0 curve appearing near $\beta_{0x} = 0$ in the case of the "meander" (the slope of the scan line is $\lambda = 1$). The influence of initial energy can be seen from Fig. 13a; ions were injected at initial phase of $t_0 = 0.25$ with

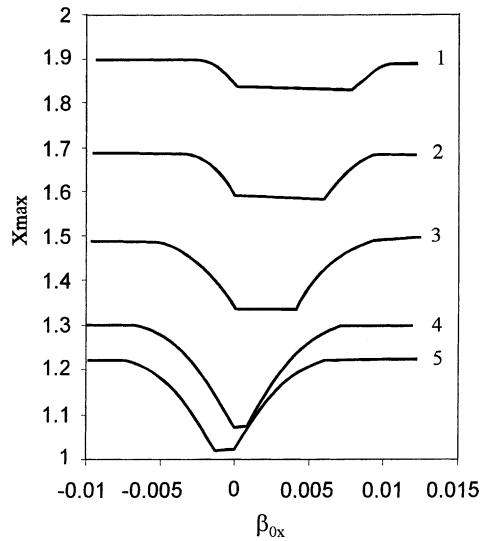

Fig. 12. The dependence of the oscillation amplitude on the stability parameter β_{0x} near the $\beta_{0x} = 0$ quasi-stability line calculated for the pulse EC-signal for different initial phases: (1) $t_0 = 0.18$; (2) $t_0 = 0.2$; (3) $t_0 = 0.22$; (4) $t_0 = 0.24$; (5) $t_0 = 0.26$. Exposure time of 300 rf cycles.

initial coordinate $x_0 = 1$. Fig. 13b shows the dips obtained for different initial coordinates; ions were injected along the X axis with initial energy of 5 eV at phase $t_0 = 0.25$; exposure time is 300 rf cycles. The influence of the exposure time on the profile of the dips is shown in Fig. 13c ($x_0 = 1$; $t_0 = 0.25$; the initial energy is 5 eV). Fig. 13d illustrates the changes in the dips depending on the initial phase at which ions are injected into the rf field ($x_0 = 1$; the initial energy is 5 eV; exposure time is 300 rf cycles). Note, that curves a3, b3, c4 and d2 in Fig. 13 are all the same.

The shapes of the dips in the amplitude vs. β_0 curve in the case of the rf voltage with harmonic waveforms are shown in Fig. 14. The influence of the injection phase on the dips near $\beta_{0z} = 0.5$ is shown in Fig. 14a for the harmonic rf voltage (ions were injected along the Z axis with initial energy of 5 eV). We see that the point corresponding to $\beta_{0z} = 0.5$ jumps from the right edge of the plateau to the left one when the phase changes. The plateau disappears at $t_0 = 0.25$. Alternatively, this effect can be described as follows: the extension of the plateau, depending on the initial

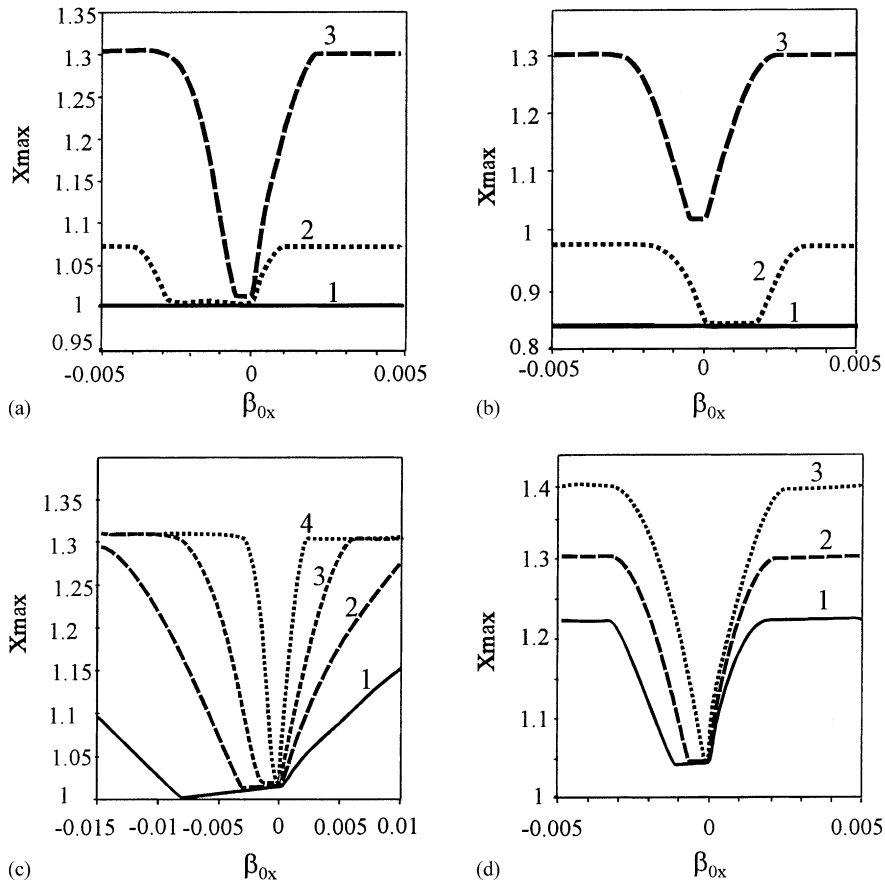

Fig. 13. The dependence of the oscillation amplitude on the stability parameter β_{0x} near the $\beta_{0x} = 0$ quasi-stability line calculated for the meander. Exposure time of 300 rf cycles: (a) initial energy: (1) 0 eV; (2) 1 eV; (3) 5 eV; (b) initial coordinate: (1) $x_0 = 0$; (2) $x_0 = 0.5$; (3) $x_0 = 1$; (c) exposure time of: (1) 20 rf cycles; (2) 50 rf cycles; (3) 100 rf cycles; (4) 300 rf cycles; (d) initial phase: (1) $t_0 = 0.24$; (2) $t_0 = 0.25$; (3) $t_0 = 0.26$.

phase, decreases and tends to zero at $t_0 = 0.25$; then it appears again but from the other side of the point $\beta_{0z} = 0.5$. The shapes of the dips near $\beta_{0z} = 0$ as a function of initial phase are shown in Fig. 14b, for the harmonic voltage and the same initial conditions. Similar to the previous case, the plateau shrinks to zero at phase $t_0 = 0.0542$, and then appears again from the other side of $\beta_{0z} = 0$. Fig. 14c shows the dips near $\beta_{0z} = -0.5$ calculated for the harmonic EC-signal (with the second harmonic). The working points lie on the scan line that corresponds to zero dc component of the rf drive voltage. Again, we see the same influence of the initial phase on the profile of the dips.

Fig. 15 shows the dips obtained for various exposure times for the case of the harmonic EC-signal (ions oscillate along the Z axis within 300 rf cycles; $\lambda = 0$; $t_0 = 0.25$). Fig. 15a demonstrates the dips near $\beta_{0z} = 0$ for ions with zero initial velocity. Fig. 15b shows the dips calculated for ions injected along the Z axis through the point $z_0 = -1$ with initial energy of 1 eV. It follows from Figs. 13 and 15 that an increase in the exposure time shortens the plateau and sharpens its edges. However, we should note here that the exposure time does not change essentially the value of the oscillation amplitude within the plateaux. Other words, the depth of the dips remains constant.

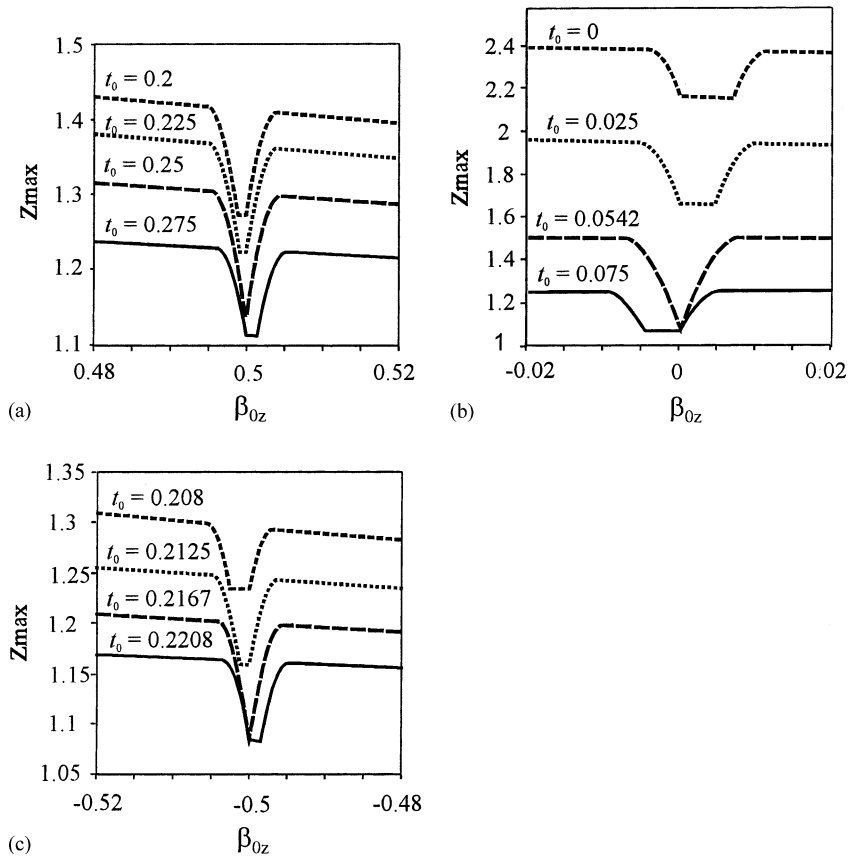

Fig. 14. The dependence of the oscillation amplitude on the stability parameter β_{0z} near quasi-stability lines for the case of the rf voltage with harmonic waveforms: (a) and (b) a simple harmonic voltage, $\beta_{0z} = 0.5$ and $\beta_{0z} = 0$ quasi-stability lines, respectively; (c) harmonic EC-signal with the second harmonic, $\beta_{0z} = -0.5$ quasi-stability line.

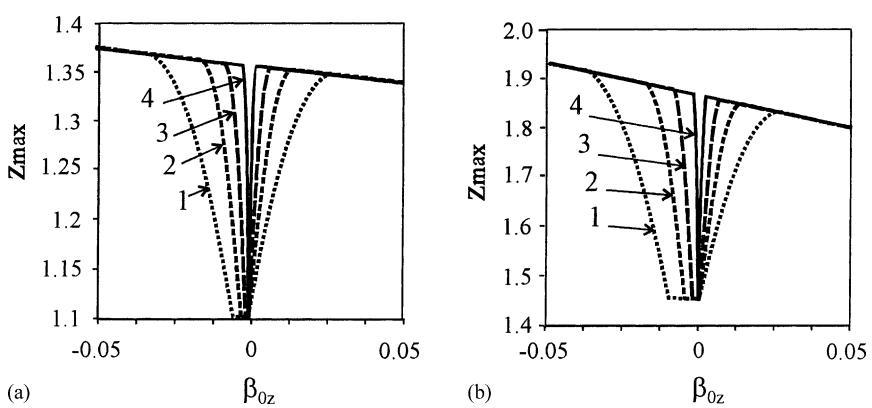

Fig. 15. The dependence of the oscillation amplitude on the stability parameter β_{0z} near the $\beta_{0z} = 0$ quasi-stability line calculated for different exposure times in the case of an harmonic EC-signal: (a) initial energy is equal to zero; (b) initial energy of 1 eV: (1) 25 rf cycles; (2) 50 rf cycles; (3) 100 rf cycles; (4) 400 rf cycles.

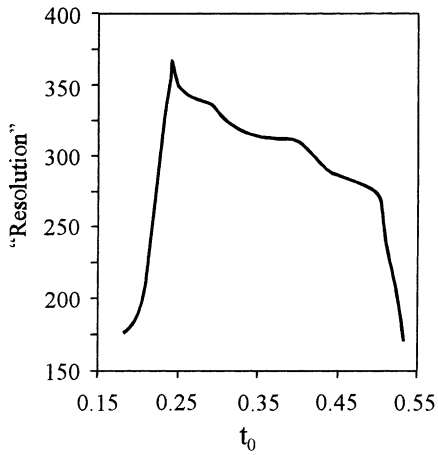

Fig. 16. "Resolution" of the dips near $\beta_{0x} = 0$ as a function of the initial phase calculated for the pulse EC-signal ($t_1 = t_2 = t_3 = t_4 = 0.25$). Exposure time of 100 rf cycles.

All the dips look like inverted peaks (in fact they represent the peaks of sensitivity). Thus, we can characterize them using a habitual term—resolution, measured, for example, at 50% peak height. Resolution of the dips near $\beta_{0x} = 0$ as a function of initial phase is shown in Fig. 16 for the pulse EC-signal ($t_1 = t_2 = t_3 = t_4 = 0.25$) for the exposure time of 100 rf cycles. The initial energy of injected ions is 5 eV. We see that even short duration sorting times yield narrow dips. This means that if the use of the mass scanning with enhanced sensitivity near quasi-stability lines yields mass peaks with high mass resolution and nearly rectangular peak shape. An increase in the exposure time to 500 rf cycles increases resolution of the dips up to 3000–5000. Theoretically, the resolution of the dips can be increased unrestrictedly by increasing exposure time, keeping the depth constant. This is an important factor for possible practical applications of this marvelous effect.

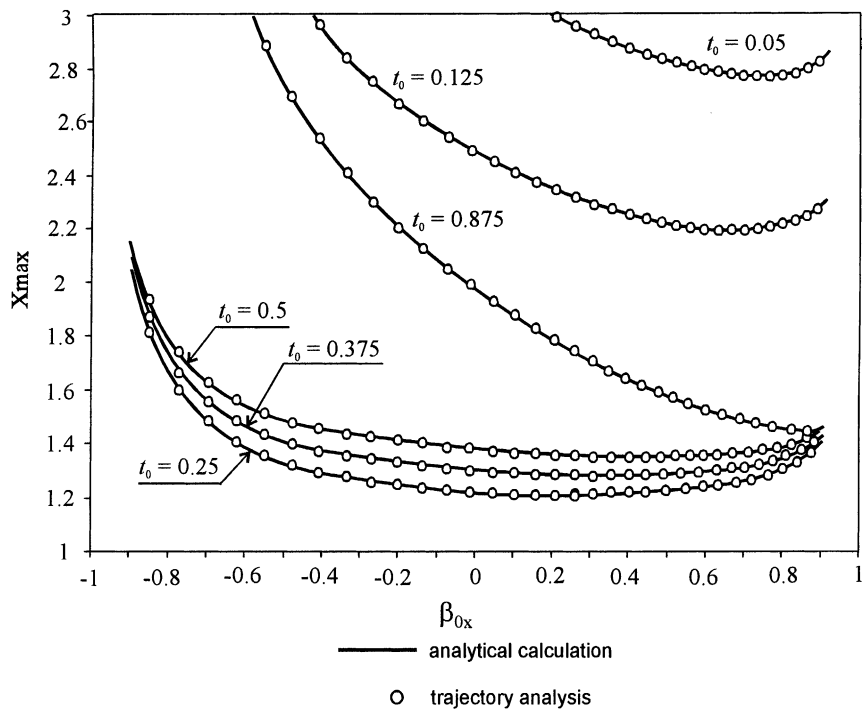

Fig. 17. The maximum ion excursion as a function of the stability parameter β_{0x} obtained for the pulse EC-signal. Solid lines represent oscillation amplitudes calculated using analytical expression (14) in Part I; datum points correspond to the amplitude determined from direct trajectory analysis. The curves are shown for the following initial phases: (1) $t_0 = 0.05$; (2) $t_0 = 0.125$; (3) $t_0 = 0.25$; (4) $t_0 = 0.375$; (5) $t_0 = 0.5$; (6) $t_0 = 0.875$.

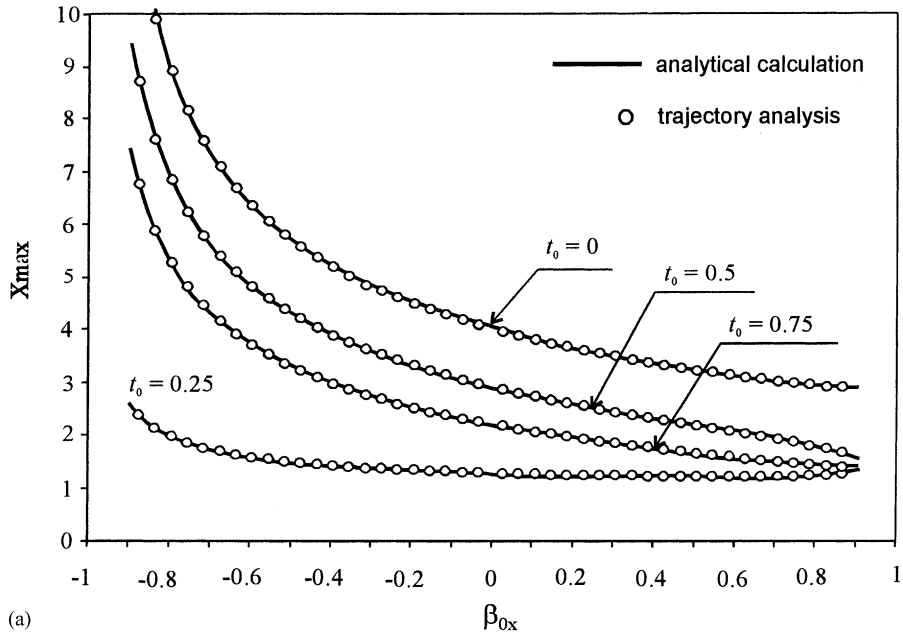

(a)

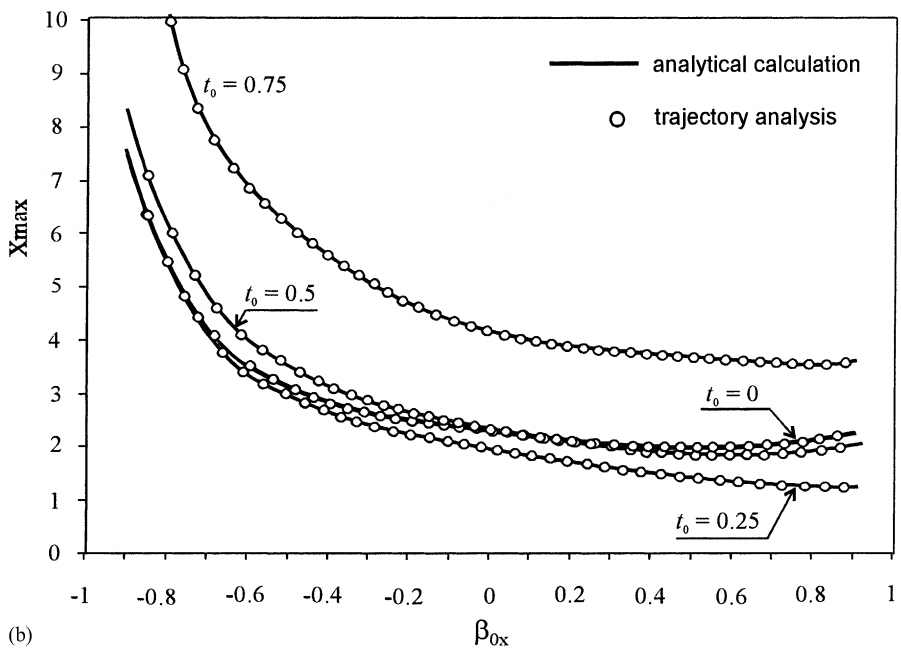

(b)

Fig. 18. The maximum ion excursion as a function of the stability parameter β_{0x}: (a) "meander", $\lambda = 1$; (b) harmonic voltage, $\lambda = 0$: (1) $t_0 = 0$; (2) $t_0 = 0.25$; (3) $t_0 = 0.5$; (4) $t_0 = 0.75$. Solid lines represent oscillation amplitudes calculated using analytical expression (14) in Part I; datum points correspond to the amplitude determined from direct trajectory analysis.

5. The smooth component of the amplitude vs. the stability parameter β_0 curve

The smooth component of the amplitude vs. the stability parameter β_0 curve is described by Eq. (14) given in Part I of this article. The correctness of this equation was verified for various waveforms of the rf drive voltage and for various initial conditions of ion motion. The validity of Eq. (14) was controlled by calculating maximum ion excursion from the origin that, in turn, was determined from a high accuracy trajectory calculation.

Fig. 17 shows the variation of the maximum ion excursion as a function of the stability parameter β_{0x} obtained for the pulse EC-signal ($t_1 = t_2 = t_3 = t_4 = 0.25$; $\lambda = 0.707106781$). The calculations were carried out for ions injected at different phases with initial energy of 5 eV along the X axis. Solid lines in this figure represent amplitudes calculated using analytical expression (14) presented in Part I; datum points on these curves correspond to amplitudes determined from trajectory analysis. These results show good agreement between analytical expression (14) and direct trajectory calculations.

Analogous dependences are shown in Fig. 18a for the "meander" ($\lambda = 1$) and Fig. 18b for the harmonic voltage ($\lambda = 0$). Disagreement between the developed theory and trajectory calculations is less than 0.1% and in most cases is less than 0.01–0.02%.

Thus, the theory of extremal characteristic solutions of the Hill equation, developed in the first part of the article, has been confirmed by direct trajectory calculations carried out in the working points both lying on quasi-stability lines and away from them.

6. Conclusions

In this article, we have shown that

- the amplitude of ion oscillations vs. the stability parameter β_0 curve exhibits some dips as a result of fine structure of the stability diagram;
- the dips appear at working points lying on quasi-stability lines;
- analytical expression (14), obtained in Part I, describes the smooth component of the amplitude vs. the stability parameter β_0 curve and is valid (with high accuracy) for various waveforms of the driving rf voltage and various initial parameters of ion motion;
- the dips in the amplitude vs. the stability parameter β_0 curve play an important role for the trapping of ions injected into the ion trap.

References

[1] E.P. Sheretov, B.I. Kolotilin, J. Tech. Phys. XII (9) (1972) 1931.
[2] E.P. Sheretov, T.B. Karnav, A.V. Brykov, Int. J. Mass Spectrom. 190/191 (1999) 113.
[3] E.P. Sheretov, V.S. Gurov, B.I. Kolotilin, Int. J. Mass Spectrom. 184 (1999) 207.
[4] E.P. Sheretov, Int. J. Mass Spectrom. 198 (2000) 83.
[5] E.P. Sheretov, B.I. Kolotilin, N.V. Veselkin, A.V. Brykov, E.V. Fedosov, Int. J. Mass Spectrom. 198 (2000) 97.
[6] E.P. Sheretov, A.E. Sheretov, in: Proceedings of the 14th International Mass Spectrometry Conference, Tampere, Finland, August, 1997, p. 230.
[7] N.W. McLachlan, Theory and Applications of Mathieu Functions, Clarendon, Oxford, 1947.
[8] E.P. Sheretov, B.I. Kolotilin, M.P. Safonov, Nonlinear resonances in hyperboloidal mass spectrometry (in Russian), Scientific Digest "Nauchnoe priborostroenie", Ryazan State Radio Technical University, Ryazan, 1995, p. 18.